Chapter 3

Results and discussion

3.1 Optimization of the HG-ICP-OES conditions

Hydride generation combined with an inductively coupled plasma optical emission spectrometry (HG-ICP-OES) was used in these experiments. The instrumental set up is shown in Figure 4. The chemicals and instrumental conditions used experiment are listed in Table 3. The instrumental conditions were optimized in order to yield an optimal signal/noise ratio. The conditions for inorganic As determination were studied. The parameters tested and fixed were wavelength, integration time, RF power, argon gas flow rate of plasma, auxiliary and carrier, concentration and flow rate of sodium borohydride ($NaBH_4$), and acidity (HCl) and flow rate of sample solution. The other parameters are linearity, detection limits and accuracy of the calibration graph. The concentration of As(III) species that was used for optimizing the parameters was 100 $\mu g\ L^{-1}$.

To achieve optimum conditions, for the emission signal following parameters were optimized.

3.1.1 Wavelength

The emission intensity of the As(III) at four wavelengths were investigated 189.0, 193.7, 197.2 and 288.8 nm and shown in Table 5 and Figure 6. The most sensitive emission wavelength was obtained at 193.7 nm. The results was in agreement with those observed by authors (Gettar *et al*., 2000 and Ng *et al*., 1998). Therefore, 193.7 nm wavelength was selected to study the next experiment.

Table 5 The relative emission signal of As(III) at various four wavelengths

As(III) wavelength (nm)	Emission intensity* x 10^4 ± %RSD
189.0	1.11 ±2.04
193.7	1.50±1.50
197.2	0.95±2.52
288.8	0.87±2.64

**5 replications*

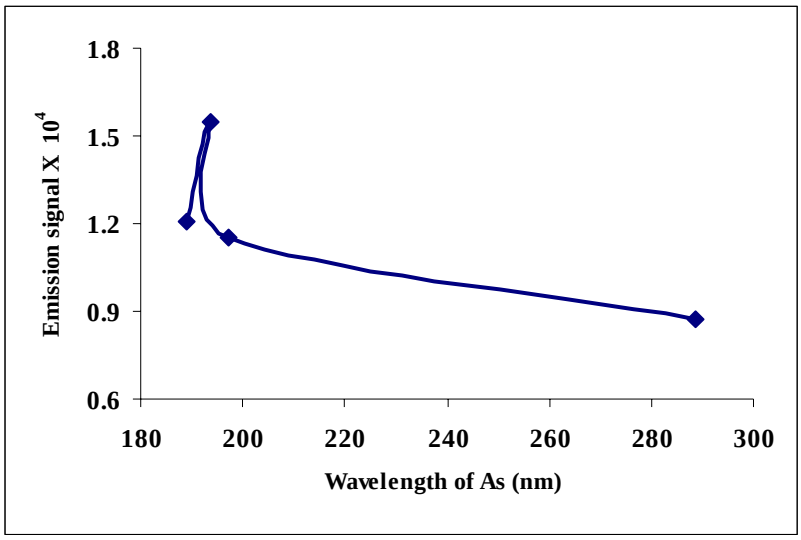

Figure 6 The relative emission signal of As(III) at various four wavelengths

3.1.2 Integration time

The integration times were varied in order to get a good integration peak. It was investigated by varying the time in the range of 1-5, 5-10, 10-20 and 20-50 seconds. The results are shown in Table 6 and Figure 7. The highest signal was obtained at 5-10 seconds. The signals were not significantly affected when compared with other integration times. This behavior was similar to that previously reported (Muller, 1999) Therefore, the integration time selected for further studies was 5-10 seconds.

Table 6 The relative emission signal of As(III) at various integration times

Integration time Min-Max.(Second)	Emission intensity* x 10^4 ± %RSD
1-5	2.84±1.24
5-10	2.98±0.62
10-20	2.83±1.12
20-50	2.82±0.85

**5 replications*

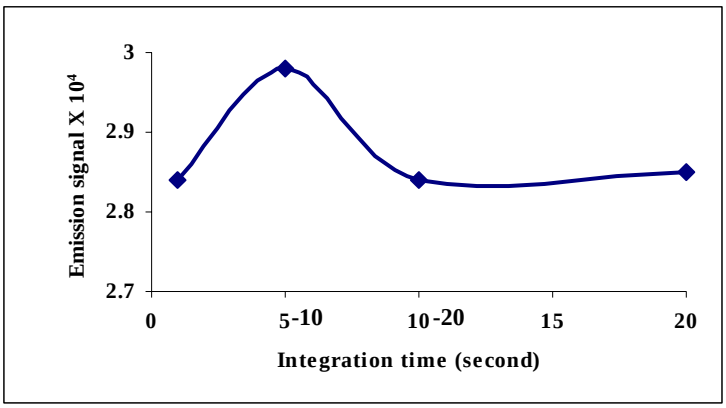

Figure 7 The relative emission signal of As(III) at various integration times

3.1.3 RF power

The radio frequency generator (RF) powers were studied in order to provide the best generation of the plasma discharge. The RF powers were investigated at 1, 1.1, 1.2, 1.3, 1.4 and 1.5 kW. The results are shown in Table 7 and Figure 8. High RF power levels can be used to increase the signal level up to about 1.5 kW. The results was in agreement previously reported (Klaue *et al.*, 1999). 1.3 kW gave the optimum signal. Because the emission signal for this power produced the least %RSD, so this power was selected for the next studies.

Table 7 The relative emission signal of As(III) at various RF powers

RF Power (kW)	Emission signal* x 10^4 ± %RSD
1	4.62±1.52
1.1	4.82±1.01
1.2	5.28±1.33
1.3	5.48±0.67
1.4	5.61±1.52
1.5	5.74±0.89

**5 replications*

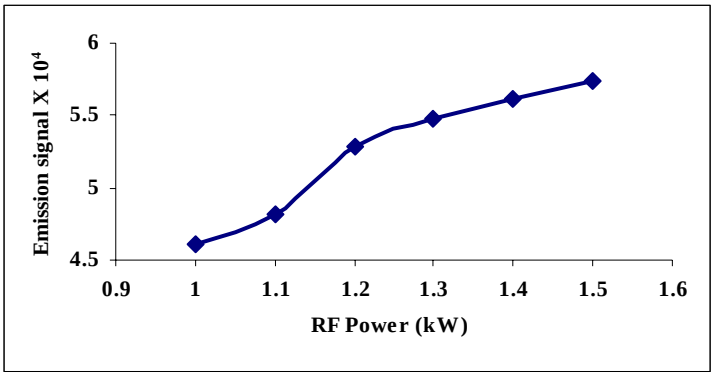

Figure 8 The relative emission signal of As(III) at various RF powers

3.1.4 Plasma gas flow rate

The plasma gas flow rates were studied by varying the range from 15 to 20 L min^{-1} with the carrier and auxiliary gas flow rates fixed. The minimum output plasma flow rate of the system is only 15 L min^{-1}. The results are shown in Table 8 and Figure 9. The emission signal decreased with an increase of the flow rate of plasma gas. The optimum emission signal was obtained at 15 L min^{-1} and then, this flow rate was selected for the next experiment.

Table 8 The relative emission signal of As(III) at various plasma gas flow rates

Plasma gas flow rate (L min^{-1})	Emission signal* x 10^4 ± %RSD
15	2.30±0.98
16	2.26±1.04
17	2.18±1.59
18	2.12±2.13
19	2.07±5.02
20	1.94±1.49

**5 replications*

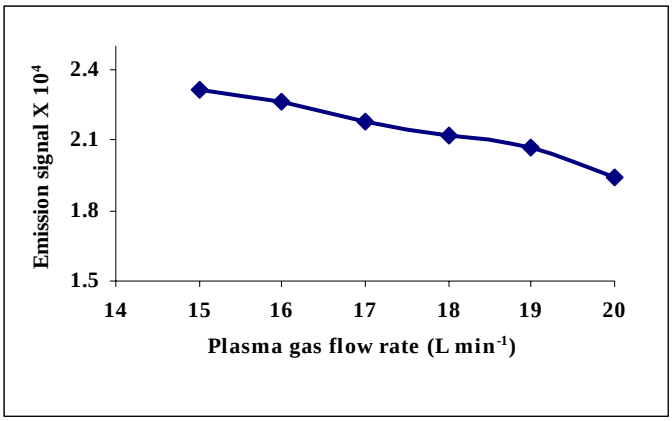

Figure 9 The relative emission signal of As(III) at various plasma gas flow rates

3.1.5 Carrier gas flow rate

Carrier gas can affect the efficiency of transference and extraction of AsH_3 from the gas-liquid separator. The carrier gas flow rate was assessed over the range of 0.1 to 0.6 L min^{-1}. The results are shown in Table 9 and Figure 10. A higher flow rate of carrier gas resulted in signal instability and decrease in sensitivity of the emission signal. This behaviour was similar to that previously reported (Gong *et al*., 2001). The highest signal was obtained at 0.3 L min^{-1} of carrier gas. This flow rate was chosen for next experiment.

Table 9 The relative emission signal of As(III) at various carrier gas flow rates

Carrier gas flow rate (L min^{-1})	Emission signal* x 10^4 ± %RSD
0.1	2.73±1.95
0.2	4.26±1.27
0.3	4.91±0.95
0.4	4.12±1.36
0.5	3.13±1.97
0.6	2.40±2.26

**5 replications*

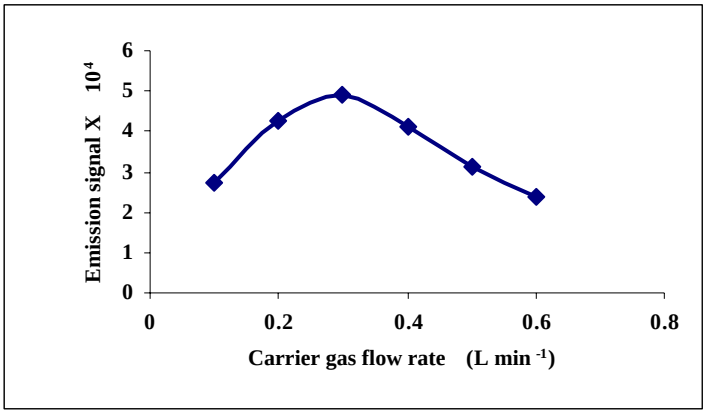

Figure 10 The relative emission signal of As(III) at various carrier gas flow rates

3.1.6 Auxiliary gas flow rate

The auxiliary gas flow rate was investigated from 0.1 to 0.6 L min^{-1}. The results are shown in Table 10 and Figure 11. The signal decreased as the flow rate of auxiliary gas was increased. A higher flow rate of auxiliary gas resulted in signal instability and a decrease in sensitivity. The signal was the highest at an auxiliary gas flow rate of 0.2 L min^{-1}. Therefore, a 0.2 L min^{-1} auxiliary gas flow rate was chosen for further experiments.

Table 10 The relative emission signal of As(III) at various auxiliary gas flow rates

Auxiliary gas flow rate (L min^{-1})	Emission signal* x 10^4 ± %RSD
0.1	5.34±1.58
0.2	5.91±1.05
0.3	5.23±2.40
0.4	5.35±2.03
0.5	5.43±2.06
0.6	5.48±2.43

**5 replications*

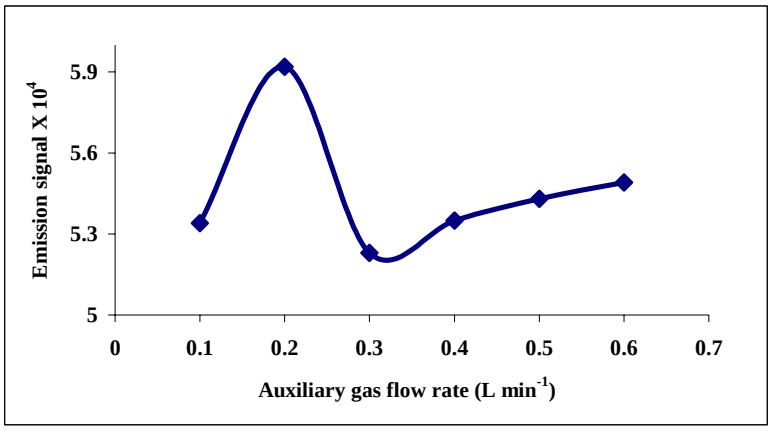

Figure 11 The relative emission signal of As(III) at various auxiliary gas flow rates

3.1.7 Pumping rates

The pumping rates were studied in order to obtain the optimum flow rate of the sample, HCl and $NaBH_4$ solutions. The results are shown in Table 11 and Figures 12-14. The emission signal increased with an increasing flow rate of sample as well as HCl and $NaBH_4$ flow rates. However, the signal was most suitable at a pumping rate of 0.5 mL min^{-1}, because of produced the lowest %RSD when compared with the other pumping rates. For the higher flow rates, the precision decreased and plasma is less stable. The flow rate of HCl and $NaBH_4$ were at least three time of sample flow rate, because of the tubing size not similar in this studied. It can be concluded that at this pumping flow rate the flow rate of the sample, HCl and $NaBH_4$ were 1.2, 0.4 and 0.4 mL min^{-1}. Therefore, this pumping flow rates were selected for the next experiments.

Table 11 The relative emission signal of As(III) at various pumping rates.

Pumping rate (mL min^{-1})	Sample flow rate (mL min^{-1})	HCl and $NaBH_4$ flow rate (mL min^{-1})	Emission signal* x 10^4 ± %RSD
0.3	0.6	0.2	2.17±1.95
0.5	1.2	0.4	3.66±1.07
0.8	3.6	1.2	4.01±2.97
1	4	1.6	4.32±2.55
1.5	6	2	5.03±2.97

**5 replications*

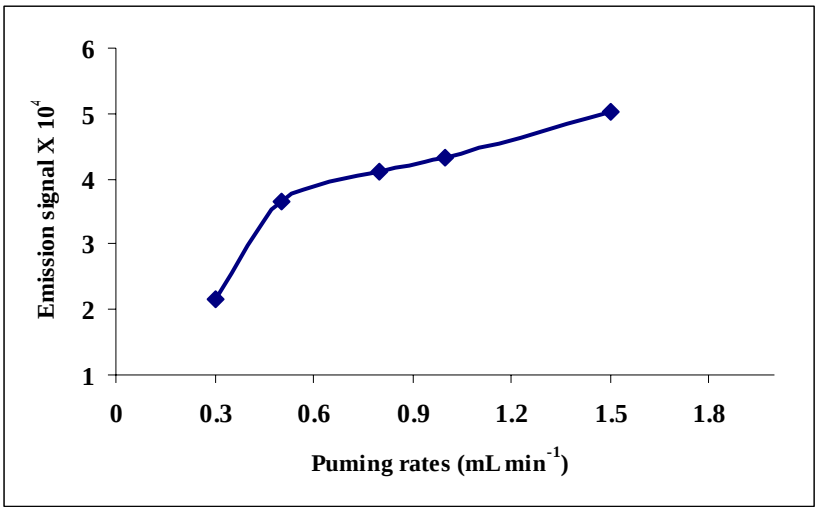

Figure 12 The relative emission signal of As(III) at various pumping rates

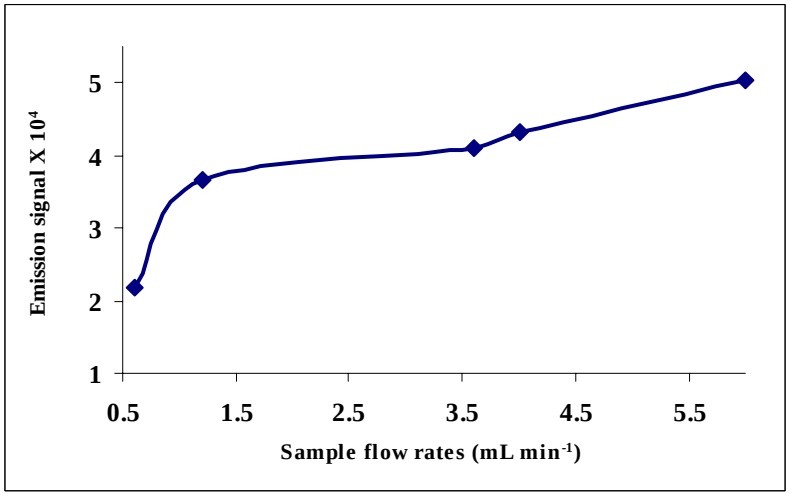

Figure 13 The relative emission signal of As(III) at various sample flow rates

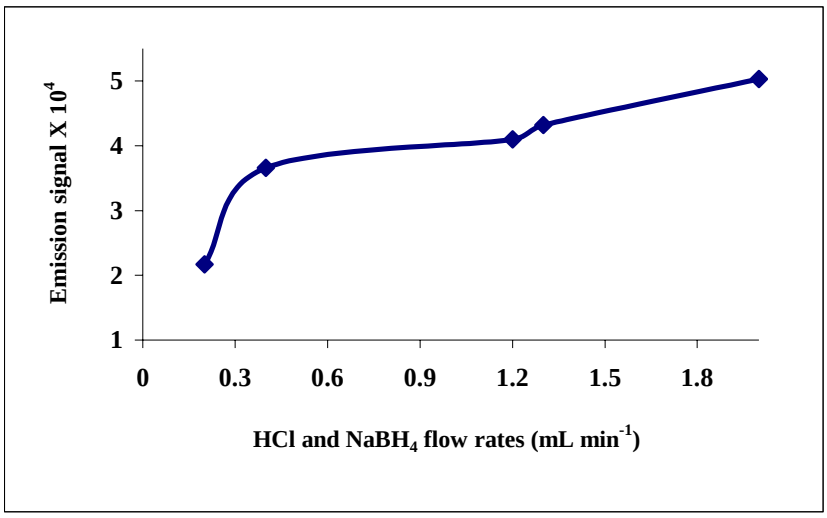

Figure 14 The relative emission signal of As(III) at various HCl and $NaBH_4$ flow rates

3.1.8 Hydrochloric acid concentration

The effect of HCl concentration used for generation of AsH_3 was investigated from 0.5 to 4 mol L^{-1} with the 0.4% (w/v) $NaBH_4$ concentration fixed. The results are expressed as emission signal *vs.* acid concentration in Table 12 and Figure 15. The emission signal rapidly increased when the HCl concentration with increased up to 2 mol L^{-1}, reaching maximum and constant value at concentration above 3 and 4 mol L^{-1}. This behaviour was similar to that previously reported. (Sigrist, 2004 and Thomson *et al.*, 1978).

The optimum concentration of HCl was 2.00 M. Because of produced the lowest %RSD. Therefore, this concentration of HCl was chosen for further experiment.

Table 12 The relative emission signal of As(III) at various HCl concentrations

HCl concentration (mol L^{-1})	Emission signal* x 10^4 ± %RSD
0.5	1.04±1.56
1	2.23±1.21
1.5	2.58±1.05
2	2.79±1.01
3	2.90±1.17
4	3.05±1.09

**5 replications*

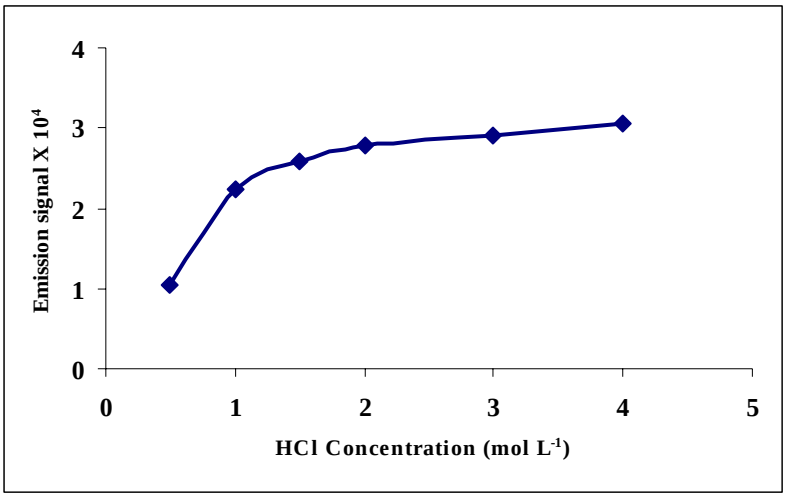

Figure 15 The relative emission signal of As(III) at various HCl concentrations

3.1.9 Reductant concentration

$NaBH_4$ was used as a reducing reagent to change arsenic to arsine gas. Therefore, the effect of $NaBH_4$ concentration was investigated at 0.1, 0.2, 0.4, 0.6, 0.8 and 1% (w/v). The results are shown in Table 13 and Figure 16. A higher signal rapidly increased when the $NaBH_4$ concentration increased up 0.1% to 0.4%, and constant value at concentration above 0.4-1%. Due to the high cost of high-purity $NaBH_4$, 0.4% was chosen as the working concentration for further experiment. The results was in agreement previously reported (Carrero *et al*., 2001).

Table 13 The relative emission signal of As(III) at various $NaBH_4$ concentrations

$NaBH_4$ concentration (%)	Emission signal* x 10^4 ± %RSD
0.1	1.51±1.23
0.2	2.31±1.20
0.3	2.97±1.59
0.4	3.46±1.96
0.8	3.57±2.45
1	3.50±3.00

**5 replications*

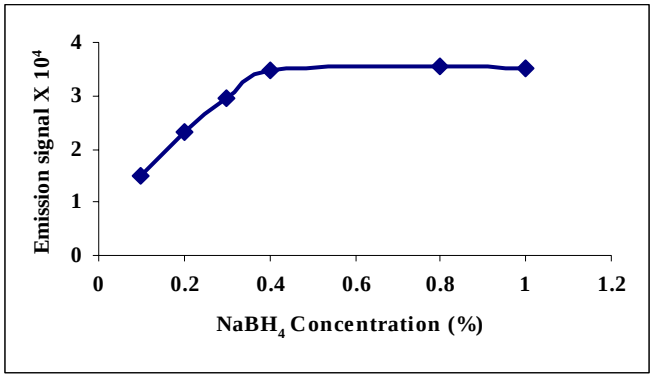

Figure 16 The relative emission signal of As(III) at various $NaBH_4$ concentrations

3.1.10 Pre-reductant concentration

The KI concentration used as a pre-reductant is one of most important parameters for reducing As(V) to As(III), by generation a more potent reducing agent than $NaBH_4$ (Aggett *et al*., 1976 and Nielsen *et at*., 1997). Table 14 and Figure 17 shows the response of various 5-60% (w/v) KI concentration. The optimum pre-reductant concentration was 40 % for 10 min, because of highest emission signal. Therefore, this concentration was selected for further experiments.

Table 14 The relative emission signal of As(III) at various KI concentrations

KI concentration (%)	Emission signal* x 10^3 ± %RSD
5	0.30±1.73
10	0.98±1.50
20	1.00±1.41
40	3.41±0.87
60	3.02±0.99

**5 replications*

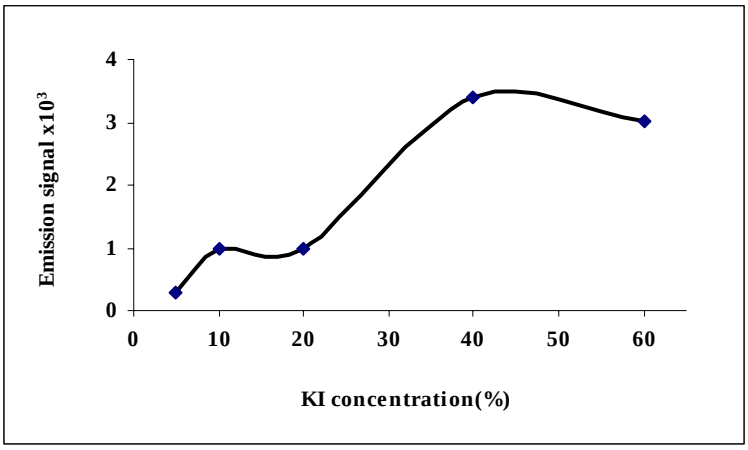

Figure 17 The relative emission signal of As(III) at various KI concentrations

3.1.11 Pre-reductant time

The reaction time for completing reduction of As(V) to As(III) was examined. Table 15 and Figure 18 show the response of the reduction time at 5 to 30 min. The optimum reduction time was 10 min and this time was used for the next experiments.

Table 15 The relative emission signal of As(III) with present for various KI times

KI time (min)	Emission signal* x 10^3 ± %RSD
5	2.30±0.73
10	3.41±0.50
20	2.07±1.01
30	1.53±1.87

**5 replications*

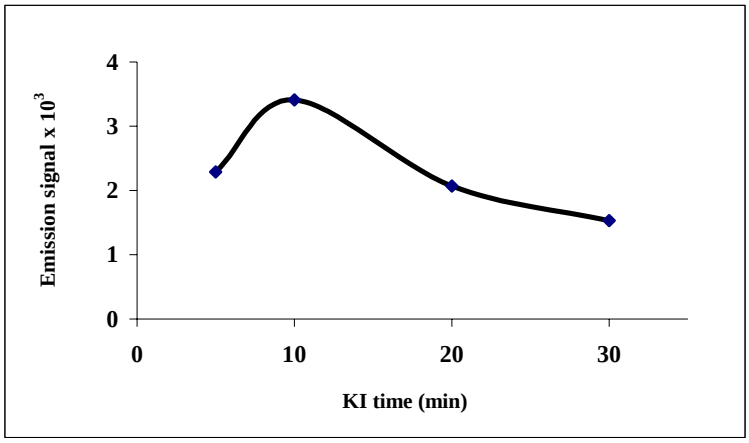

Figure 18 The relative emission signal of As(III) with present for various KI times

From this investigation the optimum conditions of the HG-ICP-OES for determination of inorganic As species are summarized in Table 16

Table 16 The optimum conditions of the HG-ICP-OES for determination of inorganic As species in this investigation.

Inductively coupled plasma optical emission spectrometer conditions	
Wavelength	193.7 nm
Measurements integration time	
Maximum	10 second
Minimum	5 second
RF power	1.3 kW.
Argon gas flow rates	
Nebulizer (Carrier gas)	0.3 L min^{-1}
Plasma	15 L min^{-1}
Auxiliary	0.2 L min^{-1}
Generator	40 MHz
Delay time	30 second
Replicates	5
Plasma viewing	axial
Hydride generation (HG) conditions	
Pumping rate	0.5 mL min^{-1}
Sample flow rate	1.2 mL min^{-1}
$NaBH_4$ and HCl flow rate	0.4 mL min^{-1}
$NaBH_4$ Concentration	0.4 % (w/v)
HCl Concentration	2 mol L^{-1}
KI Concentration	40 % (w/v)
Reduction time	10 min

3.2 Linear dynamic range

3.2.1 Linear dynamic range of total As

The emission signal response at various total As concentrations is shown in Table 17 and Figure 19 with a relative standard deviation (RSD) of less than 3% for five replicates. It was found that the optimum linear dynamic range of total As was 1-100 μg L^{-1} with a good correlation coefficient, R^2>0.9999.

Table 17 The relative emission signal response at various total As concentrations

Total As concentration (μg L^{-1})	Emission signal* x 10^3 ± %RSD
1	0.12±2.98
5	0.51±2.30
10	1.10±2.02
25	2.17±1.70
50	5.34±1.41
75	7.89±1.23
100	10.50±1.05

**5 replications*

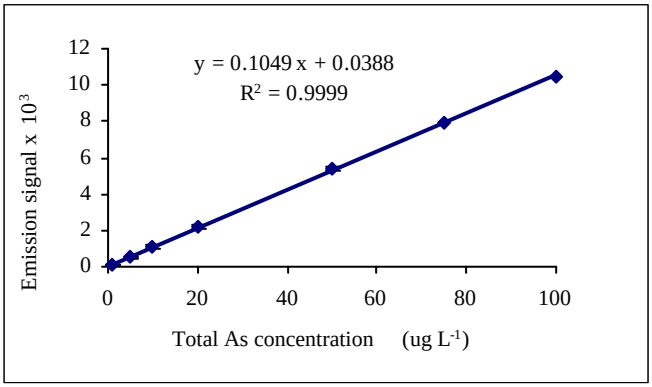

Figure 18 The calibration graph of total As concentration

3.2.2 Linear dynamic range of As(III)

Table 18 and Figure 20 show the emission signal at various As(III) concentrations giving a relative standard deviation (RSD) of less than 3% for five replicates. The results show a wide linear dynamic range of As(III) between 1-100 μg L^{-1} with a good correlation coefficient, R^2>0.9998.

Table 18 The relative emission signal at various As(III) concentrations

As(III) concentration (μg L^{-1})	Emission signal* x 10^3 ± %RSD
1	1.40±3.00
5	3.51±2.50
10	5.72±2.12
25	10.50±1.95
50	24.20±1.80
75	35.90±1.54
100	48.50±1.31

**5 replications*

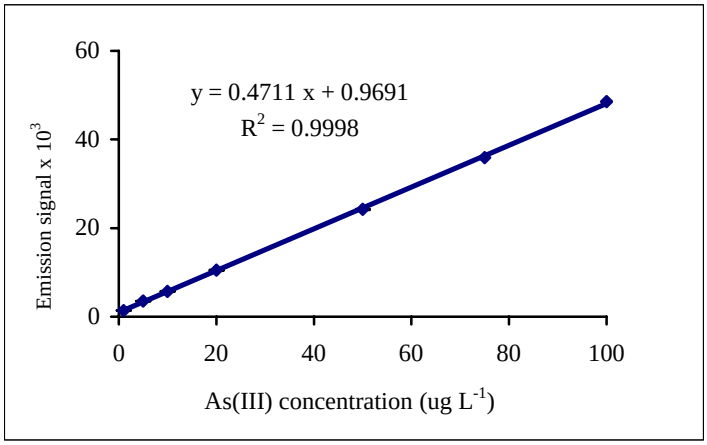

Figure 20 The calibration graph of As(III) concentrations

3.2.3 Linear dynamic range of As(V)

Table 19 and Figure 21 show the response at various As(V) concentrations with a relative standard deviation (RSD) of less than 3% for 5 replicates. The results show a wide linear dynamic range of As(V) between 1-100 μg L^{-1} with a good correlation coefficient, R^2>0.9998.

Table 19 The relative emission signal at various As(V) concentrations

As(V) concentration (μg L^{-1})	Emission signal* x 10^3 ± %RSD
1	0.19±3.00
5	0.50±2.61
10	0.99±2.10
25	1.95±1.90
50	5.80±1.61
75	7.96±1.60
100	10.50±1.25

**5 replications*

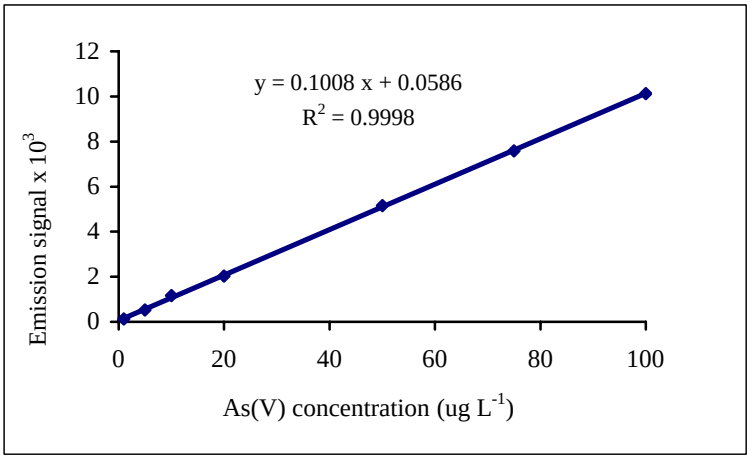

Figure 21 The calibration graph of As(V) concentrations

The linear dynamic range of three inorganic As species reaches from 1 up to 100 μg L^{-1} and covers the mostly common As concentrations in nature and also drinking water. The correlation coefficient, R^2 concerning calibration of these three inorganic As species are 0.9998-0.9999. This compares with 50 t0 200 μg L^{-1} (Gettar *et al.*, 2000) and 50 t0 100 μg L^{-1} (Wolnik *et al*, 1981).

3.3 Limit of detection and limit of quantification

The limit of detection (LOD) and limit of quantification (LOQ) of total As, As(III) and As(V) based on the calibration curve (seven standard solutions ranging from 1 to 100 μg L^{-1}, correlation coefficient R^2 = 0.9998) were tested. The limit of detection and limit of quantification were estimated from about 10 replicate peak area measurements as a concentration equivalent to three-times and ten-times (IUPAC Definition) the standard deviation of the background signal corresponding to each peak (Currie, 1999 and Taylor, 1987).

3.3.1 Limit of detection and limit of quantification total As

The total As concentrations of total As was 1 to 100 μg L^{-1} were tested with the HG-ICP-OES system. A calibration curve was then created by plotting peak area against total As concentrations. The responses are shown in Table 20, 21 and Figure 22.

Table 20 The total As concentration in blank (10 replicates)

Blank	Total As concentration in blank ($\mu g\ L^{-1}$)
1	0.020
2	0.061
3	0.063
4	0.050
5	0.064
6	0.057
7	0.045
8	0.059
9	0.046
10	0.040
Mean	0.050
SD	0.0134

Table 21 The relative emission signal at various total As concentrations

Total As concentration ($\mu g\ L^{-1}$)	Emission signal* x 10^3 ± %RSD
1	0.11±2.98
5	0.52±2.30
10	1.09±2.02
25	2.20±1.70
50	5.31±1.41
75	7.80±1.23
100	10.55±1.05

**5 replications*

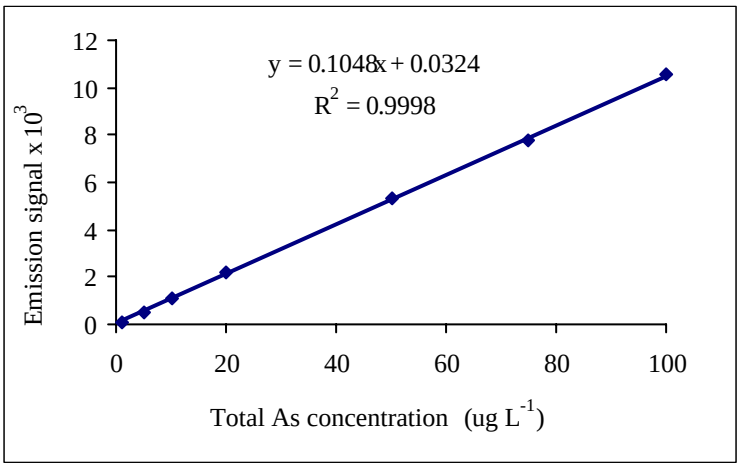

Figure 22 The calibration graph of total As concentrations

The limit of detection (3σ) for total As was calculated from the equation below:

$$C_L = kS_B / m$$

Where k = 3

$S_B = 0.0134$

$m = 0.0964$

$C_L = 3 \times 0.0134 / 0.1049$

$C_L = 0.38\ \mu g\ L^{-1}$

For, the limit of quantification (10σ) for total As was calculated from the equation below:

$$C_L = kS_B / m$$

Where k = 10

$S_B = 0.0134$

$m = 0.0964$

$C_L = 10 \times 0.0134 / 0.1049$

$C_L = 1.28\ \mu g\ L^{-1}$

Therefore, the limit of detection and limit of quantification method of total As gave a theoretical DOL of only 0.38 μg L^{-1} and LOQ of 1.28 μg L^{-1}, respectively.

3.3.2 Limit of detection and limit of quantification As(III)

The As(III) concentrations of 1 to 100 μg L^{-1} were tested with the HG-ICP-OES system. The calibration curve was then created by plotting peak area against As(III) concentrations. The responses are shown in Table 22, 23 and Figure 23.

Table 22 The As(III) concentration in blank (10 replicates)

Blank	As(III) concentration in blank (μg L^{-1})
1	0.025
2	0.035
3	0.055
4	0.040
5	0.035
6	0.045
7	0.063
8	0.041
9	0.050
10	0.036
Mean	0.043
SD	0.0111

Table 23 The relative emission signal at various As(III) concentrations

As(III) concentration (μg L^{-1})	Emission signal* x 10^3 ± %RSD
1	1.41±3.00
5	3.50±2.50
10	5.72±2.12
25	10.50±1.95
50	24.20±1.80
75	35.90±1.54
100	48.48±1.31

**5 replications*

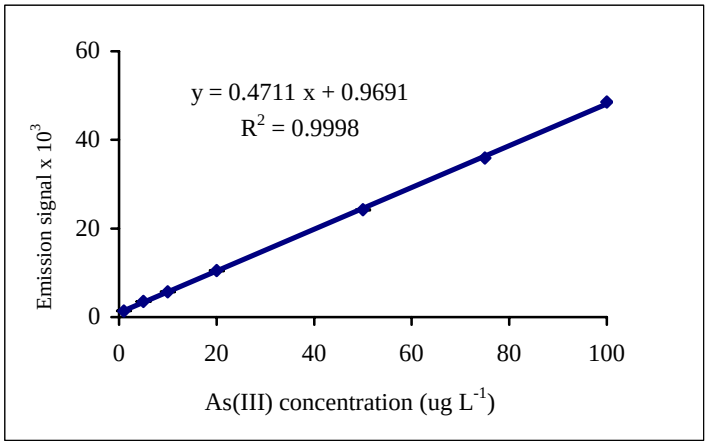

Figure 23 The calibration of As(III) concentrations

From the equation in 2.3.5, limit of detection of As(III), C_L was calculated as follow:

$$C_L = kS_B / m$$

Where k = 3

$S_B = 0.0111$

m = 0.4711

$C_L = 3 \times 0.0111 / 0.4711$

$C_L = 0.07\ \mu g\ L^{-1}$

For, the limit of quantification for As(III) was calculated from the equation below:

$$C_L = kS_B / m$$

Where k = 10

$S_B = 0.0111$

m = 0.4711

$C_L = 10 \times 0.0111 / 0.4711$

$C_L = 0.24\ \mu g\ L^{-1}$

Therefore, the limit of detection and limit of quantification method of As(III) gave a theoretical DOL of only 0.07 μg L^{-1} and LOQ of 0.24 μg L^{-1}, respectively.

The summary of the limit of detection and limit of quantification of the total As and As(III) is shown in Table 24.

Table 24 The limit of detection and limit of quantification of total As and As(III) from this investigation

As species	Limit of detection (μg L^{-1})	Limit of quantification (μg L^{-1})
Total As	0.38	1.28
As(III)	0.07	0.24

The limit of detection and limit of quantification of As(III) is 0.07 and 0.24 μg L^{-1}, respectively. These compared with previous values of 1 and 10 μg L^{-1}, respectively. (Muller, 1998), and a limit of quantification of 36 μg L^{-1} (Do *et al.*, 2000). These results indicate that the scope of the method regarding its applications to real samples will be excellent for drinking water.

3.4 Accuracy

The accuracy of this method was carried out by studying % recovery. The % recovery of total As and As(III) was performed experimentally however it % recovery of As(V) concentration was obtained by calculating the of difference between total As and As(III).

3.4.1 % Recovery of total As

Total As concentrations of 4, 8, 16 and 24 μg L^{-1} were prepared in deionized water and tested in the HG-ICP-OES system. The calibration curve was then created by plotting peak area against total As concentrations as shown in Table 25 and Figure 24. With added total As amounts of 8 and 16 μg L^{-1}. The results of 7.59 and 15.69 μg L^{-1} were equal to 94.9 and 98.1% recovery, respectively as shown in Table 28.

Table 25 The relative emission signal at various total As concentrations

Total As concentration (μg L^{-1})	Emission signal* x 10^3 ± %RSD
4	0.41±3.00
8	0.81±2.91
16	1.58±2.45
24	2.34±2.09

**5 replications*

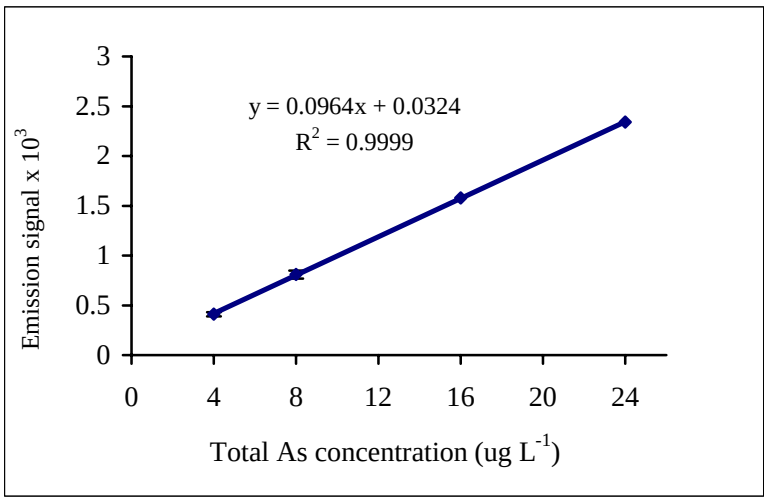

Figure 24 The calibration graph of total As concentrations

Table 26 % Recovery of total As

Added total As concentration ($\mu g\ L^{-1}$)	Found total As concentration ($\mu g\ L^{-1}$)	Recovery (%)
8	7.59	94.9
16	15.69	98.1

3.4.2 % Recovery of As(III)

As(III) concentrations of 4, 8, 16 and 24 $\mu g\ L^{-1}$ were prepared in deionized water and tested with the HG-ICP-OES system. The calibration curve was then created by plotting peak area against As(III) concentrations as shown in Table 27 and Figure 25. With added total As of 8 and 16 $\mu g\ L^{-1}$ value of 7.83 and 15.85 $\mu g\ L^{-1}$ were obtained equal to 97.9 and 99.1% recovery, respectively as shown in Table 28.

Table 27 The relative emission signal at various As(III) concentrations

As(III) concentration ($\mu g\ L^{-1}$)	Emission signal* x 10^3 ± %RSD
4	1.79±3.00
8	4.15±2.96
16	8.58±2.12
24	13.41±1.40

**5 replications*

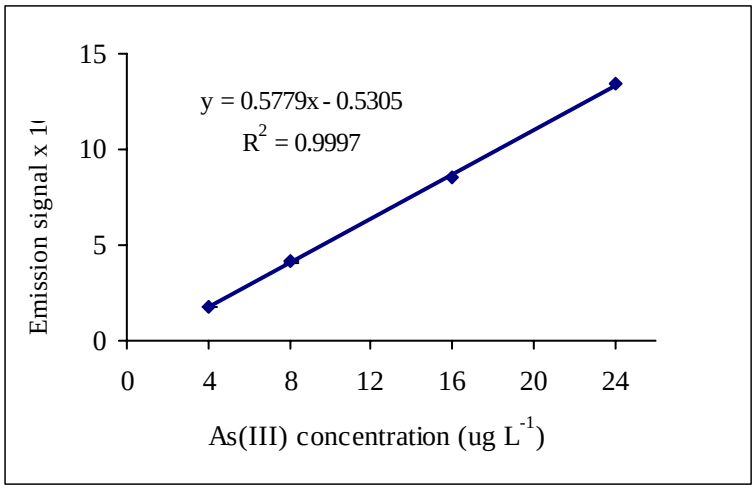

Figure 25 The calibration graph of As(III) concentrations

Table 28 % Recovery for As(III)

Added As(III) concentration ($\mu g\ L^{-1}$)	Found As(III) concentration ($\mu g\ L^{-1}$)	Recovery (%)
8	7.83	97.8
16	15.85	99.1

3.4.3 % Recovery of As(V)

The As(V) concentration was obtained by the difference between total As and As(III). From the calculation, it was found that the % recovery of As(V) was 96.9 and 98.3%, respectively as shown in Table 29.

Table 29 % Recovery of As(V)

Added total As ($\mu g\ L^{-1}$)	Found total As ($\mu g\ L^{-1}$)	Found As(III) ($\mu g\ L^{-1}$)	Found As(V) ($\mu g\ L^{-1}$)	Recovery (%)
8	7.59	3.72	3.87	96.9
16	15.69	7.83	7.86	98.3

The summary of % recovery with added the total As As(III) and As(V) concentration of 8 and 16 $\mu g\ L^{-1}$ into a blank is shown in Table 30.

Table 30 The % recovery of total As, As(III) and As(V) concentration of 8 and 16 $\mu g\ L^{-1}$ into a blank from this investigation

As species	Recovery of added 8 $\mu g\ L^{-1}$ As species into a blank (%)	Recovery of added 16 $\mu g\ L^{-1}$ As species into a blank (%)
Total As	94.9	98.1
As(III)	97.8	99.1
As(V)	96.9	98.3

The accuracy of three As species are found in the range of 94.9-99.1% recovery. The obtained results show that this method can be successfully applied to selective these three As species determination in such as natural and also drinking water samples.

3.5 Sample analysis

Drinking water samples was selected to study real samples for inorganic As determination. The five samples of drinking water were purchased from a supermarket in Had Yai, Songkhla. The quantitative analysis of total As, As(III) and As(V) was evaluated by using the calibration graph and spiking technique to check the accuracy of this method for drinking water samples.

3.5.1 Quantitative analysis of total As in drinking water

The calibration curve method was used to determine total As concentration in drinking water samples with the optimum conditions previously described in Table 16. This method is not suitable for very low concentration of total As due to the concentration of As in drinking water being below the detection limit of this investigation method as shown in Table 31.

Table 31 Total As concentration of drinking water samples determined by calibration curve method using HG-ICP-OES system with optimum conditions

Sample No.	Total As concentration ($\mu g\ L^{-1}$)
1	*n.d.*
2	*n.d.*
3	*n.d.*
4	*n.d.*
5	*n.d.*

n.d. = not-detectable

Further analysis was carried out with a calibration curve of total As at concentrations of 4, 8 and 12 $\mu g\ L^{-1}$ and then spiking at 8 and 16 $\mu g\ L^{-1}$ of total As into the drinking water samples to evaluate % recovery. The result is shown in Table 32-33.

Table 32 % Recovery of total As with spiked 8 μg L^{-1} in drinking water samples

Sample No.	Found total As conc. of spiked at 8 μg L^{-1} (μg L^{-1})	Recovery of total As at 8 μg L^{-1} (%)
1	7.50	93.8
2	7.13	89.1
3	7.36	92.0
4	6.97	87.2
5	6.90	86.3

**5 replications*

Table 33 % Recovery of total As with spiked 16 μg L^{-1} in drinking water samples

Sample No.	Found total As conc. of spiked at 16 μg L^{-1} (μg L^{-1})	Recovery of total As at 16 μg L^{-1} (%)
1	16.14	100.9
2	15.42	96.3
3	15.14	94.6
4	15.07	94.2
5	14.83	92.7

**5 replications*

The % recovery of 8 and 16 μg L^{-1} total As were in the range of 86.3-93.8 and 92.7-100.9% respectively.

3.5.2 Quantitative analysis of As(III) in drinking water

The calibration curve method was used to determine As(III) concentration in drinking water samples with the previous optimum conditions previously described in Table 16. This method is not suitable for very low

concentration of As(III) due to the concentration of As in drinking water being below the detection limit of this investigation method as shown in Table 34.

Table 34 As(III) concentration of drinking water samples determined by calibration curve method using HG-ICP-OES system with optimum conditions

Sample No.	As(III) concentration ($\mu g\ L^{-1}$)
1	*n.d.*
2	*n.d.*
3	*n.d.*
4	*n.d.*
5	*n.d.*

n.d. = not-detectable

Further analysis was carried out with the calibration curve of As(III) at concentration of 4, 8 and 12 $\mu g\ L^{-1}$ and then spiking 4, 8 and 12 $\mu g\ L^{-1}$ of As(III) into the drinking water samples to evaluate % recovery. The result is shown in Table 35-37.

Table 35 % Recovery of As(III) with spiked 4 $\mu g\ L^{-1}$ in drinking water samples

Sample No.	Found As(III) conc. of spiked at 4 $\mu g\ L^{-1}$ ($\mu g\ L^{-1}$)	Recovery of As(III) at 4 $\mu g\ L^{-1}$ (%)
1	3.73	93.2
2	3.59	89.7
3	3.93	98.2
4	3.80	95.0
5	3.61	90.1

**5 replications*

Table 36 % Recovery of As(III) with spiked 8 μg L^{-1} in drinking water samples

Sample No.	Found As(III) conc. of spiked at 8 μg L^{-1} (μg L^{-1})	Recovery of As(III) at 8 μg L^{-1} (%)
1	7.21	90.1
2	7.38	92.3
3	7.57	94.6
4	7.56	94.5
5	7.58	94.5

**5 replications*

Table 37 % Recovery of As(III) with spiked 12 μg L^{-1} in drinking water samples

Sample No.	Found As(III) conc. of spiked at 12 μg L^{-1} (μg L^{-1})	Recovery of As(III) at 12 μg L^{-1} (%)
1	11.00	91.7
2	11.01	91.8
3	11.17	93.01
4	11.06	92.2
5	10.95	91.3

**5 replications*

It was found that the % recovery of the 4, 8 and 12 μg L^{-1} spikes were in the range of 89.7-98.2, 90.1-94.6 and 91.3-93.1 % respectively.

3.6.3 Quantitative analysis of As(V)

The As(V) concentration was obtained by calculating total As –As(III). The result from Table 38 shows that the % recovery of 4 μg L^{-1} As(V) was in the range 79.4-94.3% and for 8 μg L^{-1} As(V) was in the range 90.7-111.6%.

Table 38 % Recovery of As(V) drinking water samples

Sample No.	Total As-As(III) (8-4 μg L^{-1}) =As(V) 4 μg L^{-1}*	Total As-As(III) (16-8 μg L^{-1}) =As(V) 8 μg L^{-1}*
1	7.50-3.73 = 3.77 (94.3%)	16.14-7.21 = 8.93 (111.6%)
2	7.13-3.59 = 3.54 (88.5%)	15.42-7.38 = 8.04 (100.5%)
3	7.36-3.92 = 3.44 (85.9%)	15.14-7.57 = 7.57 (94.6%)
4	6.97-3.80 = 3.17 (79.3%)	15.07-7.56 = 7.51 (93.9%)
5	6.90-3.61 = 3.29 (82.3%)	14.83-7.58 = 7.25 (90.6%)

**By calculating the total As-As(III) in Table 32-35, and 33-36, 5 replications*

The summary of three inorganic As concentrations of drinking water samples determined by standard curve method is shown in Table 39.

Table 39 Inorganic As concentrations of drinking water samples determined by standard curve method

Sample No.	Amount of As μg L^{-1}		
	Total As	As(III)	As(V)
1	*n.d.*	*n.d.*	*n.d.*
2	*n.d.*	*n.d.*	*n.d.*
3	*n.d.*	*n.d.*	*n.d.*
4	*n.d.*	*n.d.*	*n.d.*
5	*n.d.*	*n.d*	*n.d*

n.d. = not-detectable

The results was applied to determine inorganic As species in drinking water samples. As was not detected. Because the amounts of these As in drinking water samples is lower than the limit of detection of this technique, and lower than standard value in drinking water (WHO, 2003). It was found that % recovery of these As in five drinking water samples were 79.3-111.6, and then this method is high accuracy.

It can be concluded that the method established in this investigation is suitable for determination of inorganic As species because it is easy to manipulate, rapid and economic. However, this method is not applicable if the samples have very low concentrations (part per thousand billion, ηg L^{-1}), so a preconcentration method must be applied to overcome this problem.